AGU PUBLICATIONS

JGR

Journal of Geophysical Research: Space Physics

RESEARCH ARTICLE
10.1002/2017JA024078

Mars's magnetotail: Nature's current sheet laboratory

A. V. Artemyev[1,2], V. Angelopoulos[1], J. S. Halekas[3], A. Runov[1], L. M. Zelenyi[2], and J. P. McFadden[4]

[1]Department of Earth, Planetary, and Space Sciences and Institute of Geophysics and Planetary Physics, University of California, Los Angeles, California, USA, [2]Space Research Institute, RAS, Moscow, Russia, [3]Department of Physics and Astronomy, University of Iowa, Iowa City, Iowa, USA, [4]Space Sciences Laboratory, University of California, Berkeley, California, USA

Key Points:
- Configuration and plasma parameters of Mars's magnetotail current sheets
- Three types of current sheets with different pressure balances
- Comparison of current sheet properties in Mars's and Earth's magnetotails

Correspondence to:
A. V. Artemyev,
aartemyev@igpp.ucla.edu

Citation:
Artemyev, A. V., V. Angelopoulos, J. S. Halekas, A. Runov, L. M. Zelenyi, and J. P. McFadden (2017), Mars's magnetotail: Nature's current sheet laboratory, *J. Geophys. Res. Space Physics*, *122*, 5404–5417, doi:10.1002/2017JA024078.

Received 22 FEB 2017
Accepted 9 MAY 2017
Accepted article online 15 MAY 2017
Published online 24 MAY 2017

Abstract The configuration and stability of an important kinetic plasma structure, the current sheet, determine the efficiency of magnetic energy storage, release, and transport in surrounding plasmas. These properties depend on β (the ratio of plasma pressures to magnetic field pressures) and Mach number M (the ratio of bulk velocities to magnetosonic velocities). For the most investigated current sheet, the near-Earth magnetotail current sheet, these parameters fall within a relatively narrow range of values (high β, low M). To investigate current sheet behavior for a wider range of parameters, we explore current sheets in the magnetotail of Mars using Mars Atmosphere and Volatile Evolution (MAVEN) mission observations. We find that low-β, high-M current sheets are abundant in Mars's magnetotail, but high-β, low-M current sheets can also be found there. Low-β current sheets are nearly force-free, whereas high-M current sheets are balanced by a plasma flow gradient along the tail. We compare current sheet distributions in a (β, M) space for the Martian magnetotail, the near-Earth magnetotail (using Time History of Events and Macroscale Interactions during Substorms (THEMIS) mission), and the distant magnetotail (using Acceleration, Reconnection, Turbulence, and Electrodynamics of the Moon's Interaction with the Sun (ARTEMIS) mission). We also find that the pressure balance in the Martian magnetotail current sheet can occur by contributions from a wide range of ion species, or, in low beta cases, from field-aligned currents generation of a force-free magnetic field configuration. The Martian magnetotail is a natural *laboratory* where current sheet of various types can be found and investigated.

1. Introduction

One of the most intriguing and important processes in collisionless space plasmas, magnetic field energy dissipation, is controlled through the formation and destruction of intense current filaments scaling from MHD to ion kinetic regimes [*Syrovatskiĭ*, 1971; *Biskamp*, 2000; *Birn and Priest*, 2007]. In a simple planar (or 1-D) geometry, such filaments are manifested as current sheets (CSs). These universal plasma structures are observed in all planetary magnetospheres [*Jackman et al.*, 2014; *Eastwood et al.*, 2015] and in the solar wind [*Gosling*, 2012; *Mistry et al.*, 2015] and also likely abound in the solar corona [e.g., *Allanson et al.*, 2015; *Priest*, 2016, and references therein] and stellar magnetospheres [*Arons*, 2012; *Hoshino and Lyubarsky*, 2012].

Important CS properties, such as the stability and efficiency of magnetic energy transformation to plasma heating and acceleration, depend significantly on plasma parameters. The two most widely used such parameters are plasma β, the ratio of plasma pressure to magnetic field pressure, and the Mach number M, the ratio of plasma bulk velocity to fast magnetosonic velocity. Using these parameters one can categorize CSs into three groups. The first group includes CSs formed in the hot plasma of planetary magnetotails, where $\beta \gg 1$ and plasma flows are weak $M \ll 1$. In these CSs, almost all energy resides in plasma thermal pressure, and the gradients of this pressure support strong transverse diamagnetic currents that generate CSs (for models and observations, see reviews of *Schindler* [2006] and *Petrukovich et al.* [2015]). The corresponding energy release and particle heating/acceleration are caused by the instability of strong transverse currents (e.g., tearing instability, see *Coppi et al.* [1966]).

The second CS group includes solar wind and planetary magnetosheath CSs, which are characterized by large M (if plasma bulk velocity is calculated in the reference frame of the Earth bow shock), $\gg 1$ and moderate β, ~ 1. Such CSs are formed within the boundaries of plasma flows with different plasma bulk velocity directions

(or amplitudes) and closely related to the plasma flow shear [*Retinò et al.*, 2007; *Greco et al.*, 2012; *Vörös et al.*, 2016]. These boundary CSs serve as an interface for plasma flow energy transformation to particle heating [*Matthaeus et al.*, 2015]. Instabilities within these CSs are responsible for generation of electromagnetic turbulence and particle scattering, which can eventually result in plasma flow braking and shock wave formation [*Sironi and Spitkovsky*, 2011; *Hoshino and Higashimori*, 2015]. The intermediate state between CSs with $M \gg 1$, $\beta \sim 1$ (shocked and nonshocked stellar wind) and CSs with $M \ll 1$, $\beta \gg 1$ (planetary magnetotails) are represented by CSs observed in the very distant magnetotail where cold magnetosheath plasma moves into the magnetosphere [*Hoshino et al.*, 1997, 2000]. Such intermediate CSs are characterized by $M \sim 1$ and $\beta > 1$.

The third CS group includes magnetized plasma ($\beta \leq 1$) with weak ($M < 1$) flows, e.g., plasma from the solar corona [*Allanson et al.*, 2015; *Priest*, 2016] or the auroral region [*Galperin et al.*, 1986; *Chaston*, 2015, and references therein]. Such weak plasma pressure cannot generate any significant transverse currents; almost all currents are field aligned. This CS configuration is force-free ($[\mathbf{B} \times [\nabla \times \mathbf{B}]] = 0$) and can be unstable to current filamentation (some analog of the tearing instability for transverse currents [see *Galeev et al.*, 1986; *Zelenyi and Artemyev*, 2013; *Tenerani et al.*, 2015, and references therein]).

Each plasma system (e.g., Earth magnetotail) is usually characterized by a rather limited range of β and M values. Therefore, investigation of different CSs (or transformation of CSs between different groups) within one plasma system is generally impossible. Such investigation requires consideration of a variable plasma system in which boundary conditions allow observations of significant β and M parameter ranges. A good example of such systems is the induced magnetosphere of a planet without an internal magnetic field (e.g., Venus or Mars, see review by *Dubinin and Fraenz* [2015, and reference therein]). The induced magnetotail configuration contains stretched magnetic field lines with a CS embedded into a strong plasma flow [e.g., *Vaisberg and Zeleny*, 1984; *McComas et al.*, 1986; *Russell et al.*, 1992]. The absence of an internal planetary magnetic field suggests that the plasma β can reach large values in the CS's central region. Because it is essentially controlled by solar wind conditions, however, an induced magnetotail can contain twisted CSs with dominant field-aligned currents. Moreover, strong plasma flows penetrating into the induced magnetotail from the closely located magnetosheath (or formed locally through pickup and acceleration of ionospheric ions) makes CS formation with large M [e.g., *Dubinin et al.*, 1993; *Harada et al.*, 2015a] possible.

During the past decade, two missions (Mars Global Surveyor and Mars Express) have provided many important details about CSs in Mars's magnetotail (e.g., evidences of the magnetic reconnection were found, see *Eastwood et al.* [2008] and *Halekas et al.* [2009]). The simultaneous operation of the Venus Express and Mars Express spacecraft missions allows Mars and Venus magnetotails to be compared and general CS properties in induced magnetotails to be investigated [see, e.g., *Fedorov et al.*, 2008; *Dubinin and Fraenz*, 2015]. These investigations were substantially supported by information derived from global MHD simulations of Mars/Venus magnetospheres [e.g., *Kallio et al.*, 2008; *Brain et al.*, 2010; *Ma et al.*, 2015].

One of the most important properties of Mars's magnetotail is its abundance of hot heavy ions [e.g., *Fedorov et al.*, 2006; *Lundin et al.*, 2006, and references therein]. As they are accelerated significantly [*Kallio et al.*, 2006; *Lundin*, 2011; *Dubinin et al.*, 2011], these ions make an important contribution to CS configuration and pressure balance [*Dubinin and Fraenz*, 2015]. Because of the induced magnetotail's relatively small spatial scale, heavy ion dynamics is greatly influenced by the effects of magnetic field gradients (the finite gyroradius effect), and corresponding ion populations should be described using kinetic (nonfluid) approaches [e.g., *Jarvinen et al.*, 2016]. Such hot, heavy ions, being demagnetized and likely moving along Speiser trajectories [*Speiser*, 1965], are responsible for the formation of thin CSs that share many properties of CSs that exist in Earth's magnetotail: flapping motion [*Dubinin et al.*, 2012; *DiBraccio et al.*, 2015, 2017], magnetic reconnection [*Eastwood et al.*, 2008; *Halekas et al.*, 2009], and the corresponding formation of fast plasma flows [*Harada et al.*, 2015b] and plasmoids [*DiBraccio et al.*, 2015; *Hara et al.*, 2016]. Although the dynamics of CSs in Mars's magnetotail resembles that of CSs in Earth's magnetotail in many respects, peculiarities of ion content and formation mechanisms provide a much wider parameter range for Mars's magnetotail. Therefore, there is a significant interest in investigation of CSs in Mars's magnetotail.

The recently launched Mars Atmosphere and Volatile Evolution (MAVEN) spacecraft [*Jakosky et al.*, 2015] provides the first regular magnetic field and plasma parameter measurements with relatively high time resolution within Mars's magnetotail. The first results of this mission demonstrate that MAVEN instrument measurements allow probing and investigation of the magnetotail CS's fine structure [e.g., *DiBraccio et al.*, 2015; *Harada et al.*, 2015b, 2015a]. Using MAVEN observations in Mars's magnetotail, we collect statistics of CSs, derive their main

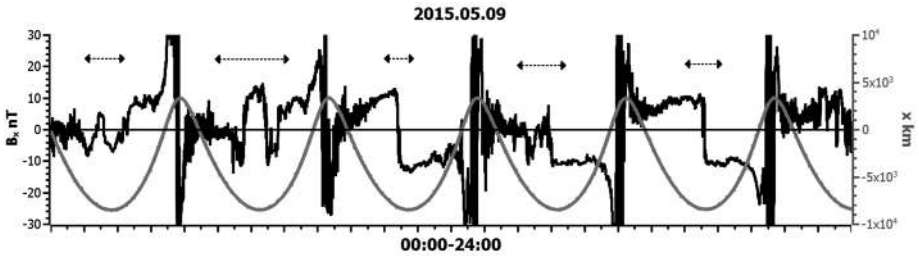

Figure 1. Magnetic field B_x and spacecraft coordinate x (in MSO coordinates) for 1 day (24 h) of observations. Arrows show time intervals of CS crossings.

characteristics, and compare them with characteristics of CSs observed in the near-Earth and lunar distance magnetotails.

2. Data Set and Methods

We consider 2 months (April and May 2015) of MAVEN observations when it visited Mars's magnetotail at about ~1–2 R_M from the planet ($R_M \approx 3400$ km). The magnetometer (MAG) on board MAVEN [*Connerney et al.*, 2015a, 2015b] provides three magnetic field components in MSO coordinates (the x axis points from Mars to the Sun, the y axis points antiparallel to Mars's orbital velocity, and the z axis completes the right-handed coordinate system). Figure 1 shows 1 day of magnetic field B_x measurements (spacecraft coordinate x is also in MSO). One can clearly distinguish sharp B_x reversals observed by MAVEN in the nightside magnetotail $x < -5000$ km. Each such reversal corresponds to a CS crossing by MAVEN. Because of CS flapping motion, there are sometimes several CS crossings within one orbit (e.g., 01:00–03:00 time interval) [*Dubinin et al.*, 2012; *DiBraccio et al.*, 2015]. To analyze such crossings, we use the MVA [*Khrabrov and Sonnerup*, 1998] coordinate system reconstructed for each crossing. In this system, B_l is directed along the maximum magnetic field variation, and B_m and B_n are magnetic field projections in the medium and minimum magnetic field variation directions. In the absence of a strong internal Mars magnetic field, B_n is presumably related to the interplanetary magnetic field into Mars's magnetotail [*Vaisberg and Zeleny*, 1984; *McComas et al.*, 1986], whereas B_m is presumably generated by local plasma currents. In the near-planet region, the crustal Mars's magnetic field also can contribute to B_n, B_m. However, if both B_m and B_n are rather small (compared with B_l magnitude) and vary slightly across the CS, then MVA can barely distinguish minimum from medium directions (the corresponding eigenvalues are very close, see details in *Sergeev et al.* [2006] and *Rong et al.* [2015]). Thus, to characterize CS configuration, we use the $B_\perp = \sqrt{B_n^2 + B_m^2}$ magnetic field averaged over the central C region ($|B_l| < 5$ nT).

For each CS crossing we gathered a time series of ion parameters measured by the Suprathermal And Thermal Ion Composition (STATIC) sensor [*McFadden et al.*, 2015], which can separate ion species. We collected density n, thermal pressure p, and bulk velocity v (magnitude of the vector velocity) for hydrogen H^+ and H_2^+, oxygen O^+ and O_2^+, and helium He^+ ions. MAVEN spacecraft is not spinning, whereas STATIC does not cover entire field of view. Therefore, there is the certain range of particle velocity distribution, which remains empty and results in uncertainty of moments calculation. The corresponding uncertainties are large when STATIC does not measure particles along the main flow direction (along Mars-Sun direction) or when plasma temperature is small (i.e., this effect would be stronger for narrow beams of cold protons and would be less pronounced for hot isotropic distributions of heavy ions). We have estimated possible underestimations of the plasma pressure that can reach 30%, whereas underestimation of the plasma bulk velocity can reach 25% of the plasma thermal velocity. To reduce influence of these uncertainties on our final conclusions, we check plasma pressure balance in observed current sheet. Moreover, to derive final conclusions we use statistical data instead of individual events.

The main contribution to the pressure and density comes from H^+, O^+, and O_2^+ [e.g., *DiBraccio et al.*, 2015; *Harada et al.*, 2015b]. We restricted our consideration to CSs with isotropic H^+, O^+, and O_2^+ thermal pressure. STATIC provides three diagonal components of the pressure tensor. We averaged each component across CSs and considered only CSs where pressure balance can be established using this averaged pressure. Therefore, for each CS crossing we have three time series of scalars n_i, p_i, $W_i = m_i v_i^2/2$ characterizing each ion species ($i = H^+, O^+, \dots$). We also calculated the total density $n_\Sigma = \sum_i n_i$, the total pressure $p_\Sigma = \sum_i p_i$, the averaged

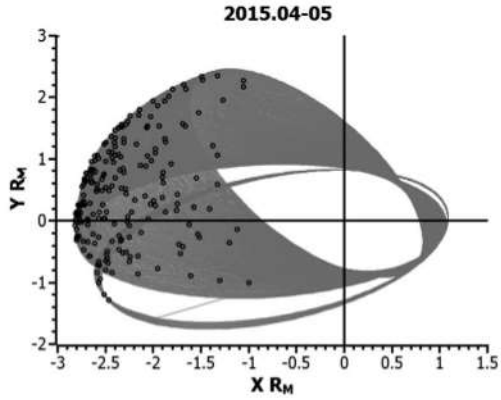

Figure 2. Spacecraft orbits (in grey) and locations of CS crossings (black circles) in the (x, y) MSO plane.

temperature $T = p_\Sigma/n_\Sigma$, and averaged kinetic energy $W=\sum_i W_i n_i/n_\Sigma$ (throughout the paper, n_i is in cm^{-3}, W and T are in keV, p_Σ is in nT^2; i.e., we used p_Σ divided by the Boltzmann constant and multiplied by $2\mu_0$). Using p_Σ, we calculated the total pressure $p_\Sigma + B_l^2 + B_n^2 + B_m^2 = B_0^2$ across the current sheet. If B_0 varies less than 20% across the CS, the vertical pressure balance (balance along the current sheet normal direction) is assumed to be established. We considered only such CS crossings.

The absence of vertical pressure balance can be caused by several factors: the contribution of hot electrons could be significant for some CSs (we included ion-dominated CSs and excluded events in which electrons can contribute to the pressure balance); significantly anisotropic plasma flows can cause uncertainties in ion pressure measurements (we restricted our consideration to isotropic cases); changes in interplanetary magnetic field orientation during CS crossings can destroy a locally 1-D CS configuration (to exclude such cases, we considered only CSs with a stably defined MVA system when the MVA vectors calculated for the time interval with $B_x>0$ coincide with the vectors calculated for the time interval with $B_x<0$). The established pressure balance criterion guarantees that none of these factors is important for the CSs we considered.

From 2 months of observations, we collected 212 CSs with an established pressure balance and isotropic thermal pressure. Only these CSs were analyzed in our study. Figure 2 shows the locations of CS crossings in MSO coordinates.

In addition to the STATIC experiment, the MAVEN spacecraft Solar Wind Ion Analyzer Inflight (SWIA) instrument [*Halekas et al.*, 2015, 2016] measures ion velocity distribution. Designed to measure solar ion flow and magnetosheath ions, this instrument does not separate ion species. Its measurements provide ion density (assuming that all ions are protons) for a relatively hot ion component (energy larger than 20 eV). We used SWIA density measurements n_{SWIA} to check STATIC measurements: n_{SWIA} should be close to n_Σ when STATIC measurements show that H^+ ions dominate and have a temperature larger than 20 eV.

Using measured ion pressures p_i, we estimated the contributions of different ions to the vertical pressure balance in CSs. The dominance of p_i in some ion species does not guarantee that these ions contribute significantly to the pressure balance, because the pressure balance corresponds to the difference Δp_i between ion pressures at the CS center and at its boundaries. We approximated ion pressures p_i by the parabolic function of B_l: $p_i=p_{i0}\left(1-\alpha_i B_l^2\right)$ and calculated p_{i0}, α_i for each CS from our data set. Coefficients $p_{0i}\alpha_i$ define relative contributions of different ion species to the pressure balance. This approximation corresponds to the pressure balance $\Sigma p_i + B_l^2 = \text{const}$ (see examples of such approximations for the Earth magnetotail CS in *Artemyev et al.* [2016]) and imitates the pressure distribution in simple CS models [e.g., *Harris*, 1962; *Harrison and Neukirch*, 2009].

To characterize the energy distribution in CSs, we used two plasma parameters: plasma β defines the ratio between plasma thermal energy and magnetic field energy, whereas Mach number defines the ratio between plasma kinetic energy and sum of plasma thermal energy and magnetic field energies. Depending on these parameters, plasma currents can be transverse to magnetic field (large β) or field aligned (small β). Small Mach number characterise magnetotail-type CSs, whereas large Mach number are more typical for CSs embedded into strong plasma flows (e.g., in the solar wind or reconnection outflows, see section 4). We calculate $\beta_{max}=\langle p_\Sigma\rangle/B_\perp^2$ and $M=\sqrt{W_\Sigma/(T+W_A)}$, where $\langle p_\Sigma\rangle$ is the total plasma pressure and $W_A=B_\perp^2/\left(2\mu_0\sum n_i m_i\right)$. Both $\langle p_\Sigma\rangle$ and W_A are averaged over the central CS region, $|B_l|<5$ nT, i.e. about 30–50% of the magnetic field amplitude (note that 5 nT is a compromise value allowing us to have several points of plasma measurements within the CS center region where plasma pressure is expected to have a maximum). We also compared β_{max}, M values derived for Mars's magnetotail CSs with the same parameters calculated for CSs in the Earth's magnetotail. To collect representative statistics of CSs (about ~100 events), we considered 3 months of Time History of Events and Macroscale Interactions during Substorms (THEMIS) C observations in 2009 in the

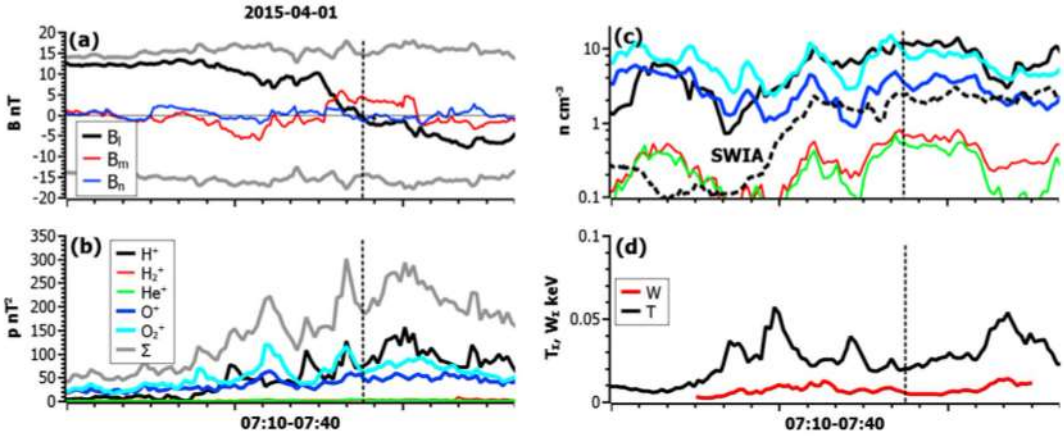

Figure 3. CS crossing with dense cold H^+, O_2^+ ions, and rarefied hot O^+ ions. Magnetic field pressure is mostly balanced by p_{H^+}. Panels show (a) magnetic field in MVA coordinates (grey curve represents the magnetic field calculated from the pressure balance $\pm B_0 = \pm\sqrt{p_\Sigma + B_l^2 + B_n^2 + B_m^2}$), (b) thermal pressures of various ion species (in nT^2), ion densities of various ion species (black dashed line represents SWIA data), (c) plasma temperature, and (d) kinetic energy. Vertical dotted lines show position of the CS center $B_l = 0$.

near-Earth tail (downtail distance ~17 Earth radii) and 1 year of Acceleration, Reconnection, Turbulence, and Electrodynamics of the Moon's Interaction with the Sun (ARTEMIS) P1 observations in the lunar distance magnetotail CS (downtail distance ~55 Earth radii). We also collect 20 CS crossings at radial distances ~180 Earth radii by ARTEMIS P2 in 2010 (this data set is limited by few month of spacecraft observations at such distances). We used spin resolution (~3 s) magnetic field measurements [*Auster et al.*, 2008] and combined measurements of plasma moments (ions and electrons) from the Electrostatic Analyzer (ESA) [*McFadden et al.*, 2008] and Solid State Telescope (SST) [e.g., *Angelopoulos et al.*, 2008] instruments. Ninety two CS crossings in the near-Earth tail and 123 CS crossings in lunar orbit with a well-established pressure balance were selected (this is only important creation for selection of CS crossings in our database). For these CSs we reconstructed the MVA coordinate system and defined the same parameters $\beta_{max} = \langle p \rangle / B_\perp^2$ and $M = \sqrt{W/(T + W_A)}$ as for the Mars's magnetotail CS (for center CS definition we use $|B_l| < 5$ nT in the near-Earth distances (THEMIS measurements) and $|B_l| < 3$ nT and lunar distances and beyond (ARTEMIS measurements)). The ESA and SST instruments on board THEMIS and ARTEMIS do not separate different ion species, and thus, p, W, and W_A were calculated under the assumption that all ions are protons. This assumption is reasonable for the Earth's magnetotail, where significant injections of oxygen ions from the ionosphere to the tail are rather rare, occurring only during strong storms.

3. CS Configurations

We present several examples of CSs from our data set. According to Figure 3, the pressure balance, which is contributed by three ion species: H^+, O^+, and O_2^+, is well established across CS, i.e., $B_0 \approx$ const. There is a clear maximum of p_{H^+} in the CS's center, whereas p_{O^+} and $p_{O_2^+}$ have wider profiles. Interestingly, the peak density value of n_{H^+} is close to the peak of density $n_{O_2^+}$, and both n_{H^+} and $n_{O_2^+}$ are much larger than n_{O^+}. Thus, comparable pressures $p_{O^+} \approx p_{O_2^+}$ mean that O^+ ions are much hotter than O_2^+ and H^+ ions. Average ion temperature T ~20–30 eV significantly larger than ion kinetic energy W. The abundance of relatively cold heavy ions results in significant underestimation of plasma density by SWIA instrument. For this CS, the maximum plasma β_{max} is about 10 and Mach number is $M < 0.3$. This CS will be included in the group of CSs typically observed in the Earth's magnetotail. Moreover, the dominance of p_{H^+} pressure makes this CS even closer to CSs in Earth's magnetotail. We note, however, that the plasma pressure in the Mars's magnetotail, ~250–300 nT^2, is provided by cold ~30 eV, very dense ~20 cm^{-3} plasma; i.e., the ion temperature is 30 times smaller and the ion density is 30 times larger than that for Earth magnetotail conditions [e.g., *Tsyganenko and Mukai*, 2003; *Wang et al.*, 2009].

Figure 4 shows a CS with an absolutely dominant heavy ion contribution to the pressure balance: $p_{O_2^+}$ is significantly larger than p_{H^+} and p_{O^+}. Such a strong $p_{O_2^+}$ is caused by a very large O_2^+ density: $n_{O_2^+}$ ~30 cm^{-3} and n_{O^+} ~15 cm^{-3}, n_{H^+} ~10 cm^{-3}. This dense ion mixture is very cold, T ~10 eV, but β_{max} and M for this CS are

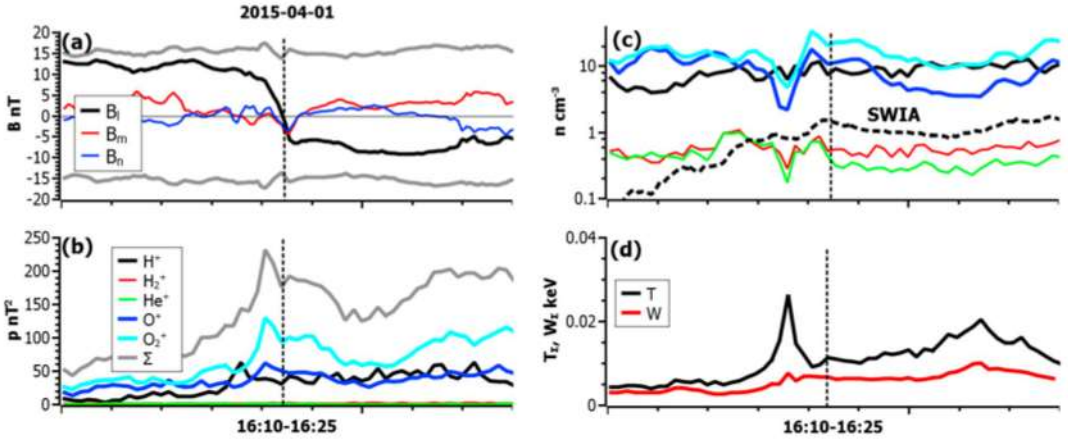

Figure 4. CS crossing with comparable densities of H^+, O^+, and O_2^+, but with O_2^+ ions much hotter than H^+, O^+ ions. Magnetic field pressure is mostly balanced by $p_{O_2^+}$. Panels are the same as in Figure 3. Vertical dotted lines show position of the CS center $B_l = 0$.

comparable with the CS parameters shown in Figure 3. The local coordinate system does not separate the B_n and B_m components well, and both these components have clear maximum at the CS's neutral plane $B_l = 0$. In contrast to the CS ion temperatures from Figure 3, the O^+ ion temperature is very close to the H^+ temperature: for both ion species (O^+ an H^+), we observe comparable densities and pressures.

Figure 5 shows a CS with absolutely dominant O^+ and O_2^+ contributions to the pressure balance. Having comparable temperatures and densities, O^+ and O_2^+ ions generate a strong pressure maximum in the CS central region. In contrast to CS densities from Figures 3 and 4, the density of H^+ exhibits a distinct decrease in the CS center and reaches maximum values at the CS boundary. Thus, we deal with a CS generated by heavy oxygen ions embedded into a hydrogen background [see observations of a similar CS configuration in *Fedorov et al.*, 2008]. The ion temperature, $T \sim 20$ eV, almost coincides with the ion kinetic energy W. Therefore, there is a very asymmetrical (in velocity space) ion velocity distribution function. Although the corresponding Mach number approaches one, $\beta_{max} \sim 3$ due to the very large B_n and B_m magnetic field components. The SWIA density profile follows the oxygen ion density profile in the central CS region, but there is an ~3 difference between total ion density and SWIA data (due to significant contributions of cold heavy ions to the plasma content).

Figure 6 shows a very hot ($T \sim 50$ eV) CS balanced by O_2^+ ions. Despite the fact that n_{H^+} and $n_{O_2^+}$ densities are comparable, hotter heavy ions totally define the plasma pressure in the CS's center. The SWIA density follows the n_{H^+} density well, especially at the CS's boundaries, where the densities of heavy ions drop significantly. Very low amplitudes of the B_n and B_m magnetic field components result in $\beta_{max} \sim 100-200$. Hot ions move

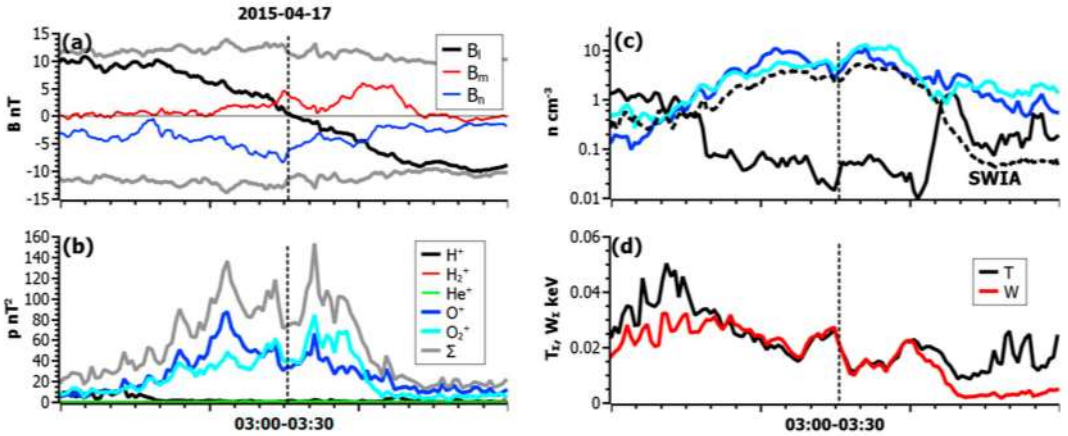

Figure 5. CS crossing almost without H^+ ions. Magnetic field pressure (B_l^2) is partially balanced by B_n, B_m maxima and by p_{O^+}, $p_{O_2^+}$ contributions. Panels are the same as in Figure 3. Vertical dotted lines show position of the CS center $B_l = 0$.

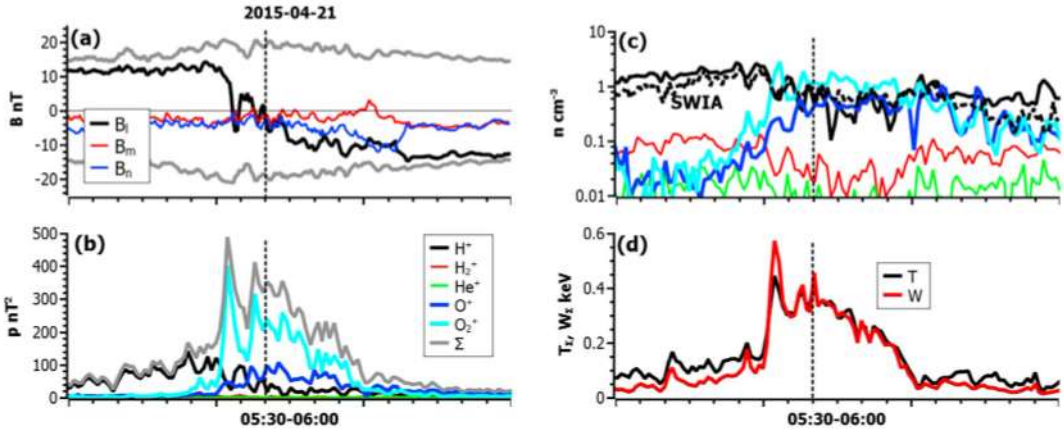

Figure 6. CS crossing with strong plasma flows ($W \sim T$). Magnetic field pressure is mostly balanced by $p_{O_2^+}$. Panels are the same as in Figure 3. Vertical dotted lines show position of the CS center $B_l = 0$.

with large bulk velocities, and the kinetic energy W coincides with T. We deal with a CS supported by a flow of hot, heavy O_2^+ ions concentrated around the CS's center. There is a strong W (and T) maximum in the CS central region. This effect can be explained by an ion acceleration mechanism in the CS without a horizontal (along the tail) pressure balance [e.g., *Dubinin et al.*, 2013, and references therein].

Figure 7 shows a CS with rather rarefied plasma (the total density reaches 10 cm^{-3}). The heavy O^+ and O_2^+ ions contribute significantly to the density, whereas n_{H^+} is 10 times smaller than $n_{O_2^+}$. The heavy ions are much colder than hydrogen ions, however, and thus the contributions of O_2^+, O^+, and H^+ to the pressure balance are comparable. The average ion temperature is about T ~20 eV. Therefore, denser heavy ions have lower temperatures and do not contribute to SWIA measurements. As a result, SWIA data coincide with the n_{H^+} profile across the entire CS. An interesting feature of this CS is the plasma pressure drop on its right side, where a strong increase in B_m offsets the plasma pressure minimum, establishing the pressure balance. This B_m peak coincides with the ion density drop (mainly due to heavy ions) and the ion temperature increase from 20 eV to 40 eV. The plasma kinetic energy is lower than the temperature, and the corresponding Mach number is much less than one.

Figure 8 shows a CS totally balanced by a local B_m increase. The ion pressure contributes very little to the CS pressure balance (mainly due to the very low ion temperature, ~3 eV). The plasma β_{max} for this CS drops to ~0.1, whereas the Mach number is much less than one (due to the small W ~1.5 eV and large Alfve'n velocity). With no ion contributions to the CS pressure balance, the CS configuration becomes force-free

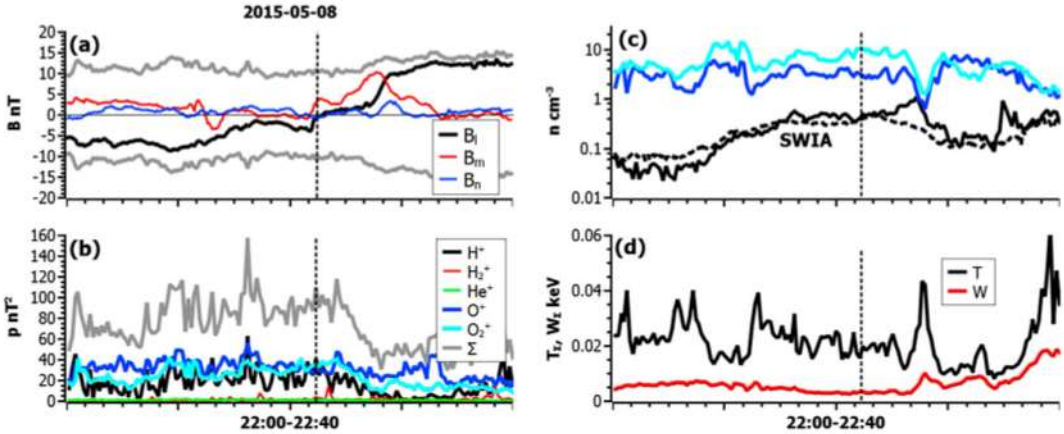

Figure 7. CS crossing with dense cold O^+, O_2^+ ions and rarefied hot H^+ ions. Magnetic field pressure is balanced by similar contributions from p_{H^+}, p_{O^+}, $p_{O_2^+}$. Panels are the same as in Figure 3. Vertical dotted lines show position of the CS center $B_l = 0$.

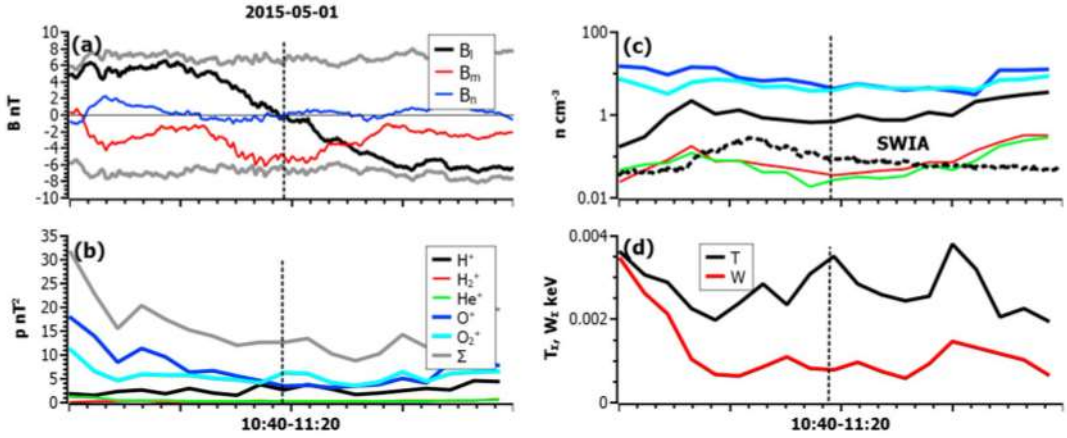

Figure 8. CS crossing with very rarefied plasma. Magnetic field pressure (B_l^2) is totally balanced by the B_m maximum without any significant contributions from ions. Panels are the same as in Figure 3. Vertical dotted lines show position of the CS center $B_l = 0$.

($B_l^2 + B_m^2 \approx$ const). The heavy ion density is much larger than the hydrogen density, but the oxygen ions are colder than the hydrogen ions (p_{O^+} and $p_{O_2^+}$ are comparable with p_{H^+}).

4. Three Groups of CSs

Figure 9 shows the distribution of CSs in a (β_{max}, M) map. Using two lines, $\beta_{max} = 10$ and $M = 1$, we can nominally separate this distribution into three groups. This separation does not assume that CSs from different groups are significantly different, because one can see that CSs occupy all sectors without distinct boundaries. However, this nominal separation allows us to discuss CS properties for different ranges of system parameters. We also note that used CS separation leaves one sector ($\beta_{max} < 10$, $M > 1$) almost empty, i.e., no CSs have small plasma pressure but strong flows. The CS distribution is also influenced by the correlation between β_{max} and M: $M \sim (1 + \beta_{max})^{-1/2}$.

Let us discuss each CS group separately. The biggest group has large $\beta_{max} > 10$ and weak plasma flows $M < 1$. CSs from this group likely represent plasma structures with strong transverse currents generated by plasma pressure gradients across the field (large β_{max} means that the plasma pressure is sufficiently large to establish the pressure balance). The absence of strong plasma flows indicates that a CS is stabilized along the tail by plasma pressure gradients (see corresponding models in *Birn et al.* [1977] and *Birn* [1979]). A CS cannot be too thin because for CSs with dominant ion diamagnetic currents [see *Schindler*, 2006, and references therein] or transient ion currents [*Burkhart et al.*, 1992; *Sitnov et al.*, 2006; *Zelenyi et al.*, 2011], the ratio of CS thickness to thermal ion gyroradius is theoretically predicted to be about the ratio of flow velocity to thermal velocity.

The group of CSs with strong plasma flows ($\beta_{max} > 10$, $M > 1$) is very interesting because such CSs could be generated in the reconnection outflow region [*Hietala et al.*, 2015, 2017; *Harada et al.*, 2015b, 2017]. Supersonic plasma flow should at last be braked within the tail at some shock wave [*Hoshino et al.*, 1997, 2000], so CSs with $M>1$ may transform into CSs with $M<1$ via flow thermalization. The generation of current density within such CSs can be organized by fast transient ions contributing to both flow and currents [*Eastwood*, 1972; *Burkhart et al.*, 1992; *Pritchett and Coroniti*, 1992; *Mingalev et al.*, 2009]. The pressure balance along the tail for these CS can be partially contributed by flow radial gradients $\partial M/\partial x$ [*Nickeler and Wiegelmann*, 2010, 2012; *Dubinin et al.*, 2013].

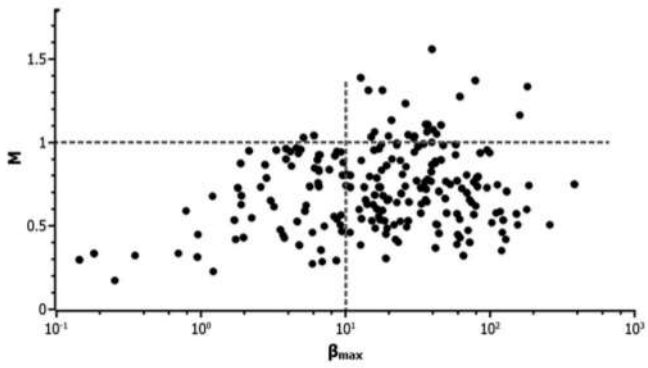

Figure 9. Distributions of CSs in (β_{max}, M) map.

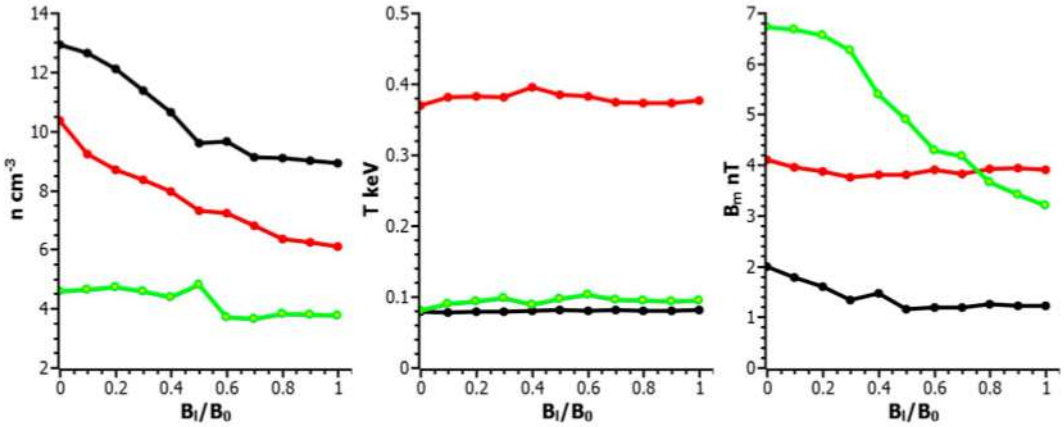

Figure 10. Averaged profiles of the plasma density, the plasma temperature, and B_m magnetic field for three CS groups: black is for $\beta_{max} > 10$, $M < 1$; red is for $\beta_{max} > 10$, $M > 1$; green is for $\beta_{max} < 10$.

The group of CSs with small plasma $\beta_{max} < 10$ is rather intriguing because the plasma pressure in such CSs is likely insufficiently large to balance the system. An alternative mechanism of CS balancing is the generation of field-aligned currents j_l supporting a local B_m maximum in the CS's central region [e.g., *Artemyev*, 2011]. Such CS are atypical in Earth's magnetotail (however, there are several examples [see *Rong et al.*, 2012; *Artemyev et al.*, 2013]) and represent magnetic field configurations where a magnetic field pressure can be larger than a plasma pressure even at the CS center $B_l \sim 0$ (i.e., β is small). In contrast to CSs with large β, small-β CSs are supported by field-aligned currents [e.g., *Harrison and Neukirch*, 2009]. Such CSs are observed in solar wind [e.g., *Haaland et al.*, 2012, and references therein] and also believed to be generated during solar flares (e.g., see discussions in *Allanson et al.* [2015] and *Wilson et al.* [2016]). Accurate investigation of such CS requires good temporal resolution of plasma measurements (unavailable for solar wind and solar corona), which can be provided for MAVEN observations (see example in Figure 8).

For the three groups of CSs we plot averaged profiles of plasma density n_Σ, temperature T_Σ, and B_m magnetic field across CSs. Figure 10 shows that although the separation is nominal, it still provides significantly different properties of CSs from different groups. For groups with large $\beta_{max} > 10$, we observe a strong plasma density maximum at the CS's center. This maximum is stronger for $M < 1$ CSs. The density of CSs with $\beta < 10$ is almost flat and does not vary across the CS. For all CSs the plasma temperature profiles do not contain any significant gradients. For both groups with $M < 1$, the plasma temperatures are similar ($T_\Sigma \sim 80$ eV), but $T_\Sigma \sim 380$ eV is much larger for CSs with $M > 1$. Thus, CSs with strong flows are also characterized by hotter ions. Those with $\beta_{max} < 10$, $M < 1$ are characterized by a bell-shaped profile of the B_m magnetic field component. Thus, our assumption that the pressure balance in these CSs is established by B_m maximum is confirmed. The average B_m is larger for CSs with strong flow than for CSs with $M < 1$, but for both CS groups $\beta_{max} > 10$, the magnetic field B_m has almost flat profiles across the CS.

5. Comparison With CSs in Earth's Magnetotail

To determine how atypical CS plasma parameters observed in the magnetotail of Mars compare with those observed in the well-investigated magnetotail of Earth, we consider THEMIS and ARTEMIS observations in the near-Earth and lunar orbit magnetotails. Figure 11 (top row) shows two examples of CSs crossed by the THEMIS C and ARTEMIS P1 spacecraft. We select typical examples of CSs with plasma parameters typical of these regions (see statistics of Earth's magnetotail CSs in *Runov et al.* [2006], *Artemyev et al.* [2011], *Petrukovich et al.* [2015], and *Artemyev et al.* [2016]). THEMIS C observed a CS with a boundary magnetic field $B_0 \sim 15$ nT comparable with data obtained for Mars's magnetotail (see Figures 3–8). This is a characteristic B_0 value for downtail distance $\sim 17\ R_E$ where THEMIS C crossed the CS (see B_0 distribution along the tail in *Tsyganenko and Mukai* [2003], *Shukhtina et al.* [2004], and *Artemyev et al.* [2016]). Therefore, the total plasma pressures in the center of a CS in Mars's magnetotail at $\sim 1\ R_M$ and Earth's magnetotail at $\sim 17\ R_E$ should be comparable. CSs in the magnetotails of Mars and Earth should have comparable β_{max} values. Ions (protons) in Earth's magnetotail are much hotter ($T \sim 2.5$ keV) than ions in Mars's magnetotail $T_\Sigma \sim 100$ eV (see Figure 10), whereas the ion density in Earth's magnetotail ($n_i \sim 0.15$ cm^{-3}) is much lower than that in Mars's magnetotail ($n_\Sigma \sim 15$ cm^{-3}).

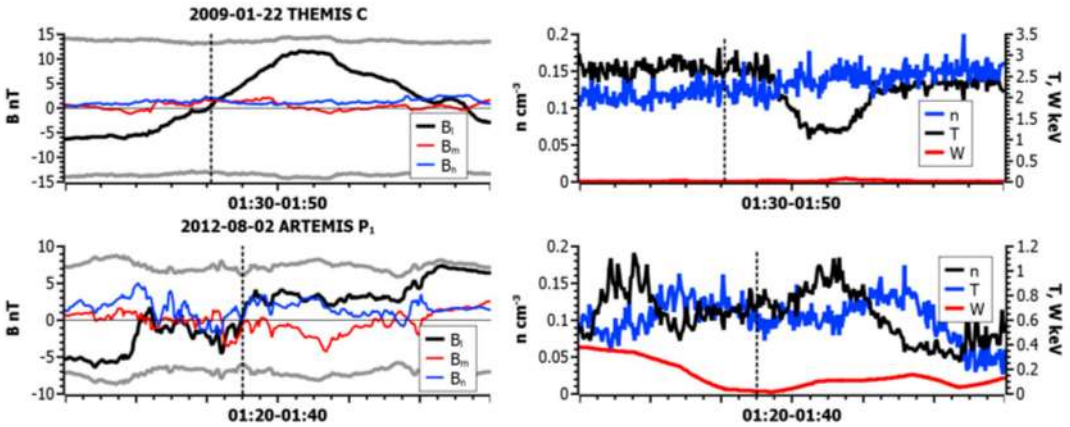

Figure 11. Two CS crossings by (top row) THEMIS and (bottom row) ARTEMIS spacecraft in the near-Earth magnetotail and at lunar distance. Vertical dotted lines show position of the CS center $B_l = 0$.

However, this example of a CS in Earth's magnetotail is characterized by a very weak plasma flow $W \ll T$, and the corresponding Mach number drops to zero. There are no such low M values in Mars's magnetotail (see Figure 9).

Because the plasma temperature and density decrease with distance from Earth, lunar orbit CSs are characterized by colder ions. Figure 11 (bottom row) shows one ARTEMIS CS crossing. Although the magnetic field magnitude, $B_0 \sim 7$ nT, is lower, the ion temperature is higher, $T \sim 700$ eV, than for Mars's magnetotail CSs (see Figures 3–8). Interestingly, the plasma kinetic energy can be significant $W/T \sim 1/3$ for distant lunar CSs, which makes the plasma parameters of these CSs closer to those in Mars's magnetotail.

Figure 11 demonstrates that CSs observed in Earth's magnetotail should have β_{max} comparable with (and Mach number lower than) β_{max} (M) in CSs observed in Mars's magnetotail. To check this assumption, we plot parameters of 93 near-Earth and 112 lunar distant magnetotail CS crossings to the (β_{max}, M) map shown in Figure 9. Figure 12 shows that CSs observed in Earth's magnetotail occupy the entire range of β_{max} values, but have much smaller M values. The lowest M values can be found for near-Earth magnetotail CSs, whereas lunar distant CSs have higher M. These three CS populations (near-Earth tail, lunar distant, and Mars's magnetotail) are well separated in M range: only several CS crossings in Earth's magnetotail have M values comparable with typical values for Mars's magnetotail. We also include 20 CSs observed far beyond the lunar orbit during ARTEMIS P2 traveling to the distant magnetotail (radial distance is about ~180 Earth radii). These CSs generally have larger M for the same β in comparison to CSs observed at the near-Earth tail and at lunar orbit. However, larger statistic is needed for more accurate comparison of these CSs and CSs found in the Mar magnetotail (such statistics can be collected using, e.g., Geotail measurements, see *Vasko et al.* [2015]).

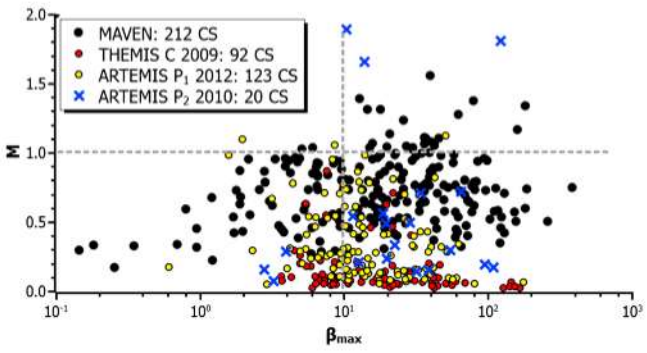

Figure 12. Distributions of CSs in the (β_{max}, M) map: black is for MAVEN data; red is for THEMIS data (downtail distance ~17 Earth radii); yellow is for ARTEMIS P1 data (2012, downtail distance ~55 Earth radii); blue crosses for ARTEMIS P2 data (2010, downtail distance ~180 Earth radii).

6. Heavy Ion Contribution

According to Figures 3–8, different ion species can contribute to CS pressure and density. Moreover, the pressure dominance of particular ion species does not necessarily mean that these ions contribute significantly to the pressure balance because the pressure balance contribution is defied by gradients, $\partial p_i / \partial B_x^2$. To study ion contributions, we replot Figure 9 and indicate the dominance of different ions by colors. Figure 13a shows that for most of CSs, oxygen (O^+, O_2^+) absolutely dominates the pressure, i.e., $p_O > 75\%$ of the total pressure. About 30% of CSs have

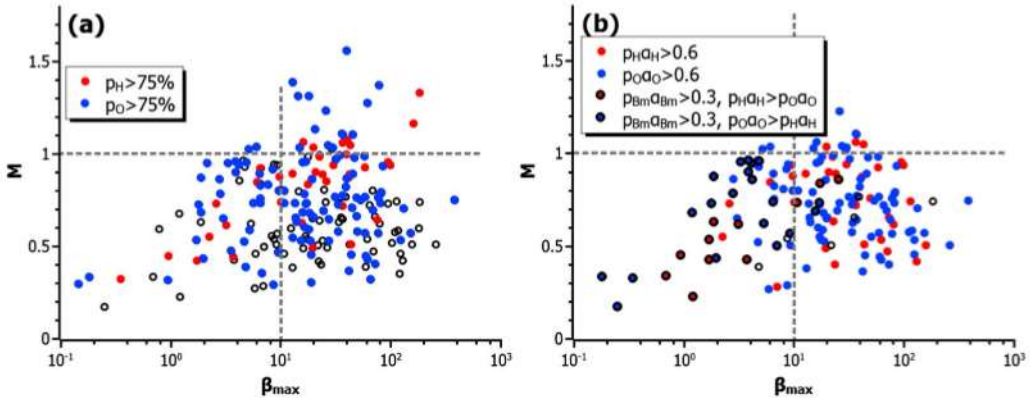

Figure 13. Distributions of CSs in the (β_{max}, M) map: colors show contributions of different ion species (a) to the pressure and (b) to the pressure balance. The index O represents the combined data for O^+ and O_2^+ ions.

significant hydrogen pressure, $p_H > 75\%$; the remainder of the data set is represented by CSs in which both oxygen and hydrogen contribute to the pressure. There is no correlation between ion species contribution to the pressure and the plasma parameters β_{max} and M. Therefore, CS separation onto three groups does not depend on ion species plasma content.

Figure 13b shows the distribution of the ion contribution to the pressure balance (we use coefficients of the pressure approximation $p_i = p_{i0}\left(1 - \alpha_i B_l^2\right)$). We separate CSs with $p_O\alpha_O > 0.6$ (where more than 60% of the pressure variation across the CS is provided by both O^+ and O_2^+), with $p_H\alpha_H > 0.6$, and with $B_{m0}^2\alpha_m > 0.3$, where B_{m0} and α_m are derived from the approximation, $B_m^2 = B_{m0}^2\left(1 - \alpha_m B_l^2\right)$. This CSs with $B_{m0}^2\alpha_m > 0.3$ correspond to a significant contribution of the B_m magnetic field component to the pressure balance. We separate this CS class into two subclasses depending on which ion species contribute the remainder of the pressure balance. One can see that CSs with $B_{m0}^2\alpha_m > 0.3$ occupy the low plasma β_{max} region. There is significant overlapping of CSs from all three classes in the (β_{max}, M) map, however. As in Figure 13a, there is no separation of CSs with $p_O\alpha_O > 0.6$ and $p_H\alpha_H > 0.6$ in the plasma parameter map.

Figure 13 shows that concentration of heavy ions and their contributions to pressure do not influence directly the CS configuration. Series of numerical simulations have demonstrated that heavy ions can significantly influence the CS thinning and following reconnection [e.g., *Shay and Swisdak*, 2004; *Karimabadi et al.*, 2011; *Markidis et al.*, 2011]. Therefore, one can expect to observe more intense cross-field currents (larger β_{max}) for CSs with larger heavy ion contributions. However, in the Mars's magnetotail we deal with the multicomponent plasma when temperatures of various ion populations are significantly different. Temperature of heavy ions is often much lower than temperature of hot (shocked solar wind) protons. Therefore, the significant heavy ion contribution to the pressure balance (and to cross-field currents) does not guarantee that the corresponding CS is really thin in comparison with the cold ion gyroradius. This could explain the absence of correlation between CS configuration and ion content. Further investigations are needed to establish the spatial distributions of currents within the Mars's magnetotail and to determine a role of heavy ions in generation of these currents.

7. Conclusions

We considered more than 200 CS crossings in Mars's magnetotail to derive the distribution of magnetic plasma parameters, β_{max} and M, and compare them with Earth magnetotail parameters. The main conclusions of this study can be summarized as follows:

1. Mars's magnetotail CSs occupy a much wider range of β_{max} and M parameters than Earth's magnetotail CSs. Although there are some lunar distance CSs with $M \sim 1$, the population of CSs with $M \geq 1$ is much better represented in Mars's magnetotail.
2. There is an interesting group of CSs with small β_{max} and a significant magnetic field shear contribution to the pressure balance. Although similar CSs have been observed in the Earth's magnetopause [e.g., *Panov et al.*, 2011, and references therein] and solar wind [*Haaland et al.*, 2012], they have been observed much more rarely in Earth's magnetotail [see *Rong et al.*, 2012].

3. There is no correlation between significant ion species contributing to plasma content and CS location in the (β_{max}, M) map. Thus, we conclude that β_{max}, M are defined by boundary conditions (e.g., solar wind) rather than by local plasma content.

Wide range of plasma parameter values in Mars's magnetotail makes this region very attractive for further investigation of how various dynamical process efficiency (magnetic reconnection, particle acceleration, etc.) depend on CS location in β_{max}, M (or, more general, on CS configuration).

Acknowledgments
We acknowledge NASA contract NAS5-02099. This work also was supported by NASA grant NNX16AF84G. The work of Z.L.M. was supported by the Russian Scientific Foundation, project 16-42-01103. We would like to thank the following people, specifically C. W. Carlson and J. P. McFadden for use of ESA data, D.E. Larson and R.P. Lin for use of SST data, K. H. Glassmeier, U. Auster, and W. Baumjohann for the use of FGM data provided under the lead of the Technical University of Braunschweig and with financial support through the German Ministry for Economy and Technology and the German Aerospace Center (DLR) under contract 50 OC 0302. THEMIS data were downloaded from http://themis.ssl.berkeley.edu/, the MAVEN data are publicly available in NASAs Planetary Data System (http://ppi.pds.nasa.gov/mission/MAVEN).

References

Allanson, O., T. Neukirch, F. Wilson, and S. Troscheit (2015), An exact collisionless equilibrium for the Force-Free Harris Sheet with low plasma beta, *Phys. Plasmas*, *22*(10), 102116, doi:10.1063/1.4934611.

Angelopoulos, V., et al. (2008), Tail reconnection triggering substorm onset, *Science*, *321*, 931–935, doi:10.1126/science.1160495.

Arons, J. (2012), Pulsar wind nebulae as cosmic pevatrons: A current sheet's tale, *Space Sci. Rev.*, *173*, 341–367, doi:10.1007/s11214-012-9885-1.

Artemyev, A. V. (2011), A model of one-dimensional current sheet with parallel currents and normal component of magnetic field, *Phys. Plasmas*, *18*(2), 022104, doi:10.1063/1.3552141.

Artemyev, A. V., A. A. Petrukovich, R. Nakamura, and L. M. Zelenyi (2011), Cluster statistics of thin current sheets in the Earth magnetotail: Specifics of the dawn flank, proton temperature profiles and electrostatic effects., *J. Geophys. Res.*, *116*, A0923, doi:10.1029/2011JA016801.

Artemyev, A. V., A. A. Petrukovich, A. G. Frank, R. Nakamura, and L. M. Zelenyi (2013), Intense current sheets in the magnetotail: Peculiarities of electron physics, *J. Geophys. Res. Space Physics*, *118*, 2789–2799, doi:10.1002/jgra.50297.

Artemyev, A. V., V. Angelopoulos, and A. Runov (2016), On the radial force balance in the quiet time magnetotail current sheet, *J. Geophys. Res. Space Physics*, *121*, 4017–4026, doi:10.1002/2016JA022480.

Auster, H. U., et al. (2008), The THEMIS fluxgate magnetometer, *Space Sci. Rev.*, *141*, 235–264, doi:10.1007/s11214-008-9365-9.

Birn, J. (1979), Self-consistent magnetotail theory—General solution for the quiet tail with vanishing field-aligned currents, *J. Geophys. Res.*, *84*, 5143–5152, doi:10.1029/JA084iA09p05143.

Birn, J., and E. R. Priest (2007), *Reconnection of Magnetic Fields: Magnetohydrodynamics and Collisionless Theory and Observations*, Cambridge Univ. Press, Cambridge, U. K.

Birn, J., R. R. Sommer, and K. Schindler (1977), Self-consistent theory of the quiet magnetotail in three dimensions, *J. Geophys. Res.*, *82*, 147–154, doi:10.1029/JA082i001p00147.

Biskamp, D. (2000), *Magnetic Reconnection in Plasmas*, Cambridge Univ. Press, Cambridge, U. K.

Brain, D., et al. (2010), A comparison of global models for the solar wind interaction with Mars, *Icarus*, *206*, 139–151, doi:10.1016/j.icarus.2009.06.030.

Burkhart, G. R., J. F. Drake, P. B. Dusenbery, and T. W. Speiser (1992), A particle model for magnetotail neutral sheet equilibria, *J. Geophys. Res.*, *97*, 13,799–13,815, doi:10.1029/92JA00495.

Chaston, C. C. (2015), Magnetic reconnection in the auroral acceleration region, *Geophys. Res. Lett.*, *42*, 1646–1653, doi:10.1002/2015GL063164.

Connerney, J. E. P., J. Espley, P. Lawton, S. Murphy, J. Odom, R. Oliversen, and D. Sheppard (2015a), The MAVEN magnetic field investigation, *Space Sci. Rev.*, *195*, 257–291, doi:10.1007/s11214-015-0169-4.

Connerney, J. E. P., J. R. Espley, G. A. DiBraccio, J. R. Gruesbeck, R. J. Oliversen, D. L. Mitchell, J. Halekas, C. Mazelle, D. Brain, and B. M. Jakosky (2015b), First results of the MAVEN magnetic field investigation, *Geophys. Res. Lett.*, *42*, 8819–8827, doi:10.1002/2015GL065366.

Coppi, B., G. Laval, and R. Pellat (1966), Dynamics of the geomagnetic tail, *Phys. Rev. Lett.*, *16*, 1207–1210, doi:10.1103/PhysRevLett.16.1207.

DiBraccio, G. A., et al. (2015), Magnetotail dynamics at Mars: Initial MAVEN observations, *Geophys. Res. Lett.*, *42*, 8828–8837, doi:10.1002/2015GL065248.

DiBraccio, G. A., et al. (2017), MAVEN observations of tail current sheet flapping at Mars, *J. Geophys. Res. Space Physics*, *122*, 4308–4324, doi:10.1002/2016JA023488.

Dubinin, E., and M. Fraenz (2015), Magnetotails of Mars and Venus, in *Magnetotails in the Solar System, Geophys. Monogr. Ser.*, vol. 207, edited by A. Keiling, C. M. Jackman, and P. A. Delamere, pp. 34–59, AGU, Washington D. C., doi:10.1002/9781118842324.ch3.

Dubinin, E., R. Lundin, O. Norberg, and N. Pissarenko (1993), Ion acceleration in the Martian tail—PHOBOS observations, *J. Geophys. Res.*, *98*, 3991–3997, doi:10.1029/92JA02233.

Dubinin, E., M. Fraenz, A. Fedorov, R. Lundin, N. Edberg, F. Duru, and O. Vaisberg (2011), Ion energization and escape on Mars and Venus, *Space Sci. Rev.*, *162*, 173–211, doi:10.1007/s11214-011-9831-7.

Dubinin, E., M. Fraenz, J. Woch, T. L. Zhang, J. Wei, A. Fedorov, S. Barabash, and R. Lundin (2012), Bursty escape fluxes in plasma sheets of Mars and Venus, *Geophys. Res. Lett.*, *39*, L01104, doi:10.1029/2011GL049883.

Dubinin, E., M. Fraenz, T. L. Zhang, J. Woch, Y. Wei, A. Fedorov, S. Barabash, and R. Lundin (2013), Plasma in the near Venus tail: Venus express observations, *J. Geophys. Res. Space Physics*, *118*, 7624–7634, doi:10.1002/2013JA019164.

Eastwood, J. P., D. A. Brain, J. S. Halekas, J. F. Drake, T. D. Phan, M. Øieroset, D. L. Mitchell, R. P. Lin, and M. Acuña (2008), Evidence for collisionless magnetic reconnection at Mars, *Geophys. Res. Lett.*, *35*, L02106, doi:10.1029/2007GL032289.

Eastwood, J. P., H. Hietala, G. Toth, T. D. Phan, and M. Fujimoto (2015), What controls the structure and dynamics of Earth's magnetosphere?, *Space Sci. Rev.*, *188*, 251–286, doi:10.1007/s11214-014-0050-x.

Eastwood, J. W. (1972), Consistency of fields and particle motion in the 'Speiser' model of the current sheet, *Planet. Space Sci.*, *20*, 1555–1568, doi:10.1016/0032-0633(72)90182-1.

Fedorov, A., et al. (2006), Structure of the Martian wake, *Icarus*, *182*, 329–336, doi:10.1016/j.icarus.2005.09.021.

Fedorov, A., et al. (2008), Comparative analysis of Venus and Mars magnetotails, *Planet. Space Sci.*, *56*, 812–817, doi:10.1016/j.pss.2007.12.012.

Galeev, A. A., M. M. Kuznetsova, and L. M. Zelenyi (1986), Magnetopause stability threshold for patchy reconnection, *Space Sci. Rev.*, *44*, 1–41, doi:10.1007/BF00227227.

Galperin, I. I., L. M. Zelenyi, and M. M. Kuznetsova (1986), Pinching of field-aligned currents as a possible mechanism for the formation of raylike auroral forms, *Kosmicheskie Issledovaniia*, *24*, 865–874.

Gosling, J. T. (2012), Magnetic reconnection in the solar wind, *Space Sci. Rev.*, *172*, 187–200, doi:10.1007/s11214-011-9747-2.

Greco, A., W. H. Matthaeus, R. D'Amicis, S. Servidio, and P. Dmitruk (2012), Evidence for nonlinear development of magnetohydrodynamic scale intermittency in the inner heliosphere, *Astrophys. J., 749*, 105, doi:10.1088/0004-637X/749/2/105.

Haaland, S., B. Sonnerup, and G. Paschmann (2012), More about arc-polarized structures in the solar wind, *Ann. Geophys., 30*, 867–883, doi:10.5194/angeo-30-867-2012.

Halekas, J. S., J. P. Eastwood, D. A. Brain, T. D. Phan, M. Øieroset, and R. P. Lin (2009), In situ observations of reconnection Hall magnetic fields at Mars: Evidence for ion diffusion region encounters, *J. Geophys. Res., 114*, A11204, doi:10.1029/2009JA014544.

Halekas, J. S., E. R. Taylor, G. Dalton, G. Johnson, D. W. Curtis, J. P. McFadden, D. L. Mitchell, R. P. Lin, and B. M. Jakosky (2015), The solar wind ion analyzer for MAVEN, *Space Sci. Rev., 195*, 125–151, doi:10.1007/s11214-013-0029-z.

Halekas, J. S., et al. (2016), Structure, dynamics, and seasonal variability of the Mars-solar wind interaction: Maven solar wind ion analyzer inflight performance and science results, *J. Geophys. Res. Space Physics, 122*, 547–578, doi:10.1002/2016JA023167.

Hara, T., et al. (2016), MAVEN observations of magnetic flux ropes with a strong field amplitude in the Martian magnetosheath during the ICME passage on 8 March 2015, *Geophys. Res. Lett., 43*, 4816–4824, doi:10.1002/2016GL068960.

Harada, Y., et al. (2015a), Marsward and tailward ions in the near-Mars magnetotail: MAVEN observations, *Geophys. Res. Lett., 42*, 8925–8932, doi:10.1002/2015GL065005.

Harada, Y., et al. (2015b), Magnetic reconnection in the near-Mars magnetotail: MAVEN observations, *Geophys. Res. Lett., 42*, 8838–8845, doi:10.1002/2015GL065004.

Harada, Y., et al. (2017), Survey of magnetic reconnection signatures in the Martian magnetotail with MAVEN, *J. Geophys. Res. Space Physics, 122*, doi:10.1002/2017JA023952. in press.

Harris, E. G. (1962), On a plasma sheet separating regions of oppositely directed magnetic field, *Nuovo Cimento, 23*, 115–123.

Harrison, M. G., and T. Neukirch (2009), One-dimensional Vlasov-Maxwell equilibrium for the force-free Harris sheet, *Phys. Rev. Lett., 102*, 135003, doi:10.1103/PhysRevLett.102.135003.

Hietala, H., J. F. Drake, T. D. Phan, J. P. Eastwood, and J. P. McFadden (2015), Ion temperature anisotropy across a magnetotail reconnection jet, *Geophys. Res. Lett., 42*, 7239–7247, doi:10.1002/2015GL065168.

Hietala, H., A. V. Artemyev, and V. Angelopoulos (2017), Ion dynamics in magnetotail reconnection in the presence of density asymmetry, *J. Geophys. Res. Space Physics, 122*, 2010–2023, doi:10.1002/2016JA023651.

Hoshino, M., and K. Higashimori (2015), Generation of Alfvénic waves and turbulence in reconnection jets, *J. Geophys. Res. Space Physics, 120*, 3715–3727, doi:10.1002/2014JA020520.

Hoshino, M., and Y. Lyubarsky (2012), Relativistic reconnection and particle acceleration, *Space Sci. Rev., 173*, 521–533, doi:10.1007/s11214-012-9931-z.

Hoshino, M., Y. Saito, T. Mukai, A. Nishida, S. Kokubun, and T. Yamamoto (1997), Origin of hot and high speed plasmas in plasma sheet: Plasma acceleration and heating due to slow shocks, *Adv. Space Res., 20*, 973–982, doi:10.1016/S0273-1177(97)00505-X.

Hoshino, M., T. Mukai, I. Shinohara, Y. Saito, and S. Kokubun (2000), Slow shock downstream structure in the magnetotail, *J. Geophys. Res., 105*, 337–348, doi:10.1029/1999JA900426.

Jackman, C. M., et al. (2014), Large-scale structure and dynamics of the magnetotails of Mercury, Earth, Jupiter and Saturn, *Space Sci. Rev., 182*, 85–154, doi:10.1007/s11214-014-0060-8.

Jakosky, B. M., et al. (2015), The Mars atmosphere and volatile evolution (MAVEN) mission, *Space Sci. Rev., 195*, 3–48, doi:10.1007/s11214-015-0139-x.

Jarvinen, R., D. A. Brain, and J. G. Luhmann (2016), Dynamics of planetary ions in the induced magnetospheres of Venus and Mars, *Planet. Space Sci., 127*, 1–14, doi:10.1016/j.pss.2015.08.012.

Kallio, E., A. Fedorov, E. Budnik, S. Barabash, R. Jarvinen, and P. Janhunen (2008), On the properties of O^+ and O_2^+ ions in a hybrid model and in Mars Express IMA/ASPERA-3 data: A case study, *Planet. Space Sci., 56*, 1204–1213, doi:10.1016/j.pss.2008.03.007.

Kallio, E., et al. (2006), Energisation of O^+ and O_2^+ ions at Mars: An analysis of a 3-D quasi-neutral hybrid model simulation, *Space Sci. Rev., 126*, 39–62, doi:10.1007/s11214-006-9120-z.

Karimabadi, H., V. Roytershteyn, C. G. Mouikis, L. M. Kistler, and W. Daughton (2011), Flushing effect in reconnection: Effects of minority species of oxygen ions, *Planet Space Sci., 59*, 526–536, doi:10.1016/j.pss.2010.07.014.

Khrabrov, A. V., and B. U. Ö. Sonnerup (1998), Error estimates for minimum variance analysis, *J. Geophys. Res., 103*, 6641–6652, doi:10.1029/97JA03731.

Lundin, R. (2011), Ion acceleration and outflow from Mars and Venus: An overview, *Space Sci. Rev., 162*, 309–334, doi:10.1007/s11214-011-9811-y.

Lundin, R., et al. (2006), Ionospheric plasma acceleration at Mars: ASPERA-3 results, *Icarus, 182*, 308–319, doi:10.1016/j.icarus.2005.10.035.

Ma, Y. J., et al. (2015), MHD model results of solar wind interaction with Mars and comparison with MAVEN plasma observations, *Geophys. Res. Lett., 42*, 9113–9120, doi:10.1002/2015GL065218.

Markidis, S., et al. (2011), Kinetic simulations of magnetic reconnection in presence of a background O^+ population, *J. Geophys. Res., 116*, A00K16, doi:10.1029/2011JA016429.

Matthaeus, W. H., M. Wan, S. Servidio, A. Greco, K. T. Osman, S. Oughton, and P. Dmitruk (2015), Intermittency, nonlinear dynamics and dissipation in the solar wind and astrophysical plasmas, *Philos. Trans. R. Soc. A, 373*(2041), 20140154, doi:10.1098/rsta.2014.0154.

McComas, D. J., H. E. Spence, C. T. Russell, and M. A. Saunders (1986), The average magnetic field draping and consistent plasma properties of the Venus magnetotail, *J. Geophys. Res., 91*, 7939–7953, doi:10.1029/JA091iA07p07939.

McFadden, J. P., C. W. Carlson, D. Larson, M. Ludlam, R. Abiad, B. Elliott, P. Turin, M. Marckwordt, and V. Angelopoulos (2008), The THEMIS ESA plasma instrument and in-flight calibration, *Space Sci. Rev., 141*, 277–302, doi:10.1007/s11214-008-9440-2.

McFadden, J. P., et al. (2015), MAVEN SupraThermal and Thermal Ion Compostion (STATIC) instrument, *Space Sci. Rev., 195*, 199–256, doi:10.1007/s11214-015-0175-6.

Mingalev, O. V., I. V. Mingalev, K. V. Malova, L. M. Zelenyi, and A. V. Artem'ev (2009), Asymmetric configurations of a thin current sheet with a constant normal magnetic field component, *Plasma Phys. Rep., 35*, 76–83, doi:10.1134/S1063780X09010097.

Mistry, R., J. P. Eastwood, T. D. Phan, and H. Hietala (2015), Development of bifurcated current sheets in solar wind reconnection exhausts, *Geophys. Res. Lett., 42*, 10,513–10,520, doi:10.1002/2015GL066820.

Nickeler, D. H., and T. Wiegelmann (2010), Thin current sheets caused by plasma flow gradients in space and astrophysical plasma, *Ann. Geophys., 28*, 1523–1532, doi:10.5194/angeo-28-1523-2010.

Nickeler, D. H., and T. Wiegelmann (2012), Relation between current sheets and vortex sheets in stationary incompressible MHD, *Ann. Geophys., 30*, 545–555, doi:10.5194/angeo-30-545-2012.

Panov, E. V., A. V. Artemyev, R. Nakamura, and W. Baumjohann (2011), Two types of tangential magnetopause current sheets: Cluster observations and theory, *J. Geophys. Res., 116*, A12204, doi:10.1029/2011JA016860.

Petrukovich, A. A., A. V. Artemyev, I. Y. Vasko, R. Nakamura, and L. M. Zelenyi (2015), Current sheets in the Earth magnetotail: Plasma and magnetic field structure with Cluster project observations, *Space Sci. Rev.*, *188*, 311–337, doi:10.1007/s11214-014-0126-7.

Priest, E. (2016), MHD structures in three-dimensional reconnection, in *Magnetic Reconnection, Astrophys. and Space Sci. Lib.*, vol. 427, edited by W. Gonzalez and E. Parker, pp. 101–142, Springer, Switzerland, doi:10.1007/978-3-319-26432-5-3.

Pritchett, P. L., and F. V. Coroniti (1992), Formation and stability of the self-consistent one-dimensional tail current sheet, *J. Geophys. Res.*, *97*, 16,773–16,787, doi:10.1029/92JA01550.

Retinò, A., D. Sundkvist, A. Vaivads, F. Mozer, M. André, and C. J. Owen (2007), In situ evidence of magnetic reconnection in turbulent plasma, *Nat. Phys.*, *3*, 236–238, doi:10.1038/nphys574.

Rong, Z. J., et al. (2012), Profile of strong magnetic field B_y component in magnetotail current sheets, *J. Geophys. Res.*, *117*, A06216, doi:10.1029/2011JA017402.

Rong, Z. J., S. Barabash, G. Stenberg, Y. Futaana, T. L. Zhang, W. X. Wan, Y. Wei, X. D. Wang, L. H. Chai, and J. Zhong (2015), The flapping motion of the Venusian magnetotail: Venus Express observations, *J. Geophys. Res. Space Physics*, *120*, 5593–5602, doi:10.1002/2015JA021317.

Runov, A., et al. (2006), Local structure of the magnetotail current sheet: 2001 Cluster observations, *Ann. Geophys.*, *24*, 247–262.

Russell, C. T., M. Ong, J. G. Luhmann, K. Schwingenschuh, W. Riedler, and E. Eroshenko (1992), Bow shocks and magnetotails of Venus and Mars—A comparison, *Adv. Space Res.*, *12*, 163–167, doi:10.1016/0273-1177(92)90329-V.

Schindler, K. (2006), *Physics of Space Plasma Activity*,Cambridge Univ. Press, Cambridge, U. K., doi:10.2277/0521858976.

Sergeev, V. A., D. A. Sormakov, S. V. Apatenkov, W. Baumjohann, R. Nakamura, A. V. Runov, T. Mukai, and T. Nagai (2006), Survey of large-amplitude flapping motions in the midtail current sheet, *Ann. Geophys.*, *24*, 2015–2024.

Shay, M. A., and M. Swisdak (2004), Three-species collisionless reconnection: Effect of O^+ on magnetotail reconnection, *Phys. Rev. Lett.*, *93*, 175001.

Shukhtina, M., N. Dmitrieva, and V. Sergeev (2004), Quantitative magnetotail characteristics for different magnetospheric states, *Ann. Geophys.*, *22*, 1019–1032, doi:10.5194/angeo-22-1019-2004.

Sironi, L., and A. Spitkovsky (2011), Acceleration of particles at the termination shock of a relativistic striped wind, *Astrophys. J.*, *741*, 39, doi:10.1088/0004-637X/741/1/39.

Sitnov, M. I., M. Swisdak, P. N. Guzdar, and A. Runov (2006), Structure and dynamics of a new class of thin current sheets, *J. Geophys. Res.*, *111*, A08204, doi:10.1029/2005JA011517.

Speiser, T. W. (1965), Particle trajectories in model current sheets: 1. Analytical solutions, *J. Geophys. Res.*, *70*, 4219–4226, doi:10.1029/JZ070i017p04219.

Syrovatskiĭ, S. I. (1971), Formation of current sheets in a plasma with a frozen-in strong magnetic field, *Sov. J. Exp. Theor. Phys.*, *33*, 933.

Tenerani, A., M. Velli, A. F. Rappazzo, and F. Pucci (2015), Magnetic reconnection: Recursive current sheet collapse triggered by ideal tearing, *Astrophys. J. Lett.*, *813*, L32, doi:10.1088/2041-8205/813/2/L32.

Tsyganenko, N. A., and T. Mukai (2003), Tail plasma sheet models derived from Geotail particle data, *J. Geophys. Res.*, *108*(A3), 1136, doi:10.1029/2002JA009707.

Vaisberg, O. L., and L. M. Zeleny (1984), Formation of the plasma mantle in the Venusian magnetosphere, *Icarus*, *58*, 412–430, doi:10.1016/0019-1035(84)90087-3.

Vasko, I. Y., A. A. Petrukovich, A. V. Artemyev, R. Nakamura, and L. M. Zelenyi (2015), Earth's distant magnetotail current sheet near and beyond lunar orbit, *J. Geophys. Res. Space Physics*, *120*, 8663–8680, doi:10.1002/2015JA021633.

Vörös, Z., E. Yordanova, M. M. Echim, G. Consolini, and Y. Narita (2016), Turbulence-generated proton-scale structures in the terrestrial magnetosheath, *Astrophys. J. Lett.*, *819*, L15, doi:10.3847/2041-8205/819/1/L15.

Wang, C., L. R. Lyons, R. A. Wolf, T. Nagai, J. M. Weygand, and A. T. Y. Lui (2009), Plasma sheet $PV^{5/3}$ and nV and associated plasma and energy transport for different convection strengths and AE levels, *J. Geophys. Res.*, *114*, A00D02, doi:10.1029/2008JA013849.

Wilson, F., T. Neukirch, M. Hesse, M. G. Harrison, and C. R. Stark (2016), Particle-in-cell simulations of collisionless magnetic reconnection with a non-uniform guide field, *Phys. Plasmas*, *23*, 032302, doi:10.1063/1.4942939.

Zelenyi, L., and A. Artemyev (2013), Mechanisms of spontaneous reconnection: From magnetospheric to fusion plasma, *Space Sci. Rev.*, *178*, 441–457.

Zelenyi, L. M., H. V. Malova, A. V. Artemyev, V. Y. Popov, and A. A. Petrukovich (2011), Thin current sheets in collisionless plasma: Equilibrium structure, plasma instabilities, and particle acceleration, *Plasma Phys. Rep.*, *37*, 118–160, doi:10.1134/S1063780X1102005X.